Increasing the Dimensionality of Soft Proofing: Gloss

Alexis Gatt*, Raja Bala†, Stephen Westland* and Phil Green‡
****Centre for Colour Design Technology, University of Leeds, Leeds, UK***
†Xerox, Rochester, New York, USA
‡London College of Communications, London, UK

Abstract

The purpose of this study is to improve the accuracy of soft proofing by increasing the amount of information rendered on screen. We present a workflow that extends traditional colorimetry beyond simple color appearance prediction to a higher dimensional representation, which includes gloss. The intention is to provide a full goniometric simulation of the spatial distribution of light reflected by a print (BRDF) based upon data gathered with simple and inexpensive instruments, glossmeters and spectrophotometers. The proposed workflow is essentially an extended version of standard color characterization models. Instead of providing a single output (CIE XYZ), the workflow estimates the entire distribution of reflected colors under all possible angles (BRDFs of CIE X, Y and Z). An empirical analysis of a large set of goniophotometer measurements has been used to unveil the key characteristics of prints' BRDFs. Finding an accurate mapping between these parameters and color and gloss measurements constitutes the main focus of this article. By using existing color and gloss characterization models, BRDFs of CIE X, Y and Z channels can be obtained from simple CMYK data using this workflow. Its overall accuracy is finally quantitatively assessed and judged to be of good quality.

Introduction

Color management has greatly matured over the last decade to the point that proofing, i.e. assessing the acceptability of the finished piece, can now be performed effectively on monitors, a process termed soft proofing. Soft proofing systems are now claimed to give a closer colorimetric approximation to the actual final output than conventional hard copy proofing systems [1]. Nevertheless, it is a common experience that color experts in industries such as Graphic Arts do not always agree that a colorimetric match is a good predictor of an appearance match.

While viewing conditions have been investigated and standardized [2,3], the effect of differences in substrate properties such as texture and finish on color appearance have been less intensively studied. In fact, given the complexity inherent in the perception of color, it was only natural that the problem was initially simplified to the study of simple stimuli, assumed to be near-perfect Lambertian diffusers, viewed and illuminated under restricted geometries specially designed to avoid more complex phenomena. However, this simplified approach continues to form the basis of current state-of-the-art color management systems, and it should thus come as no surprise that such methods break down, at least partially, when employed in industrial applications, where the higher dimensionality of light and matter interactions become inevitable.

In this context, the purpose of this study is to improve the accuracy of soft proofing by increasing the amount of information rendered on screen. Ultimately, the aim is to provide an interactive computer-based simulation faithfully rendering the total appearance of printer paper illuminated by the viewing booths typically employed in prepress houses. This first implies enhancing materials simulation beyond simple color appearance prediction to more complete representations, including gloss and texture. As the title suggests, providing an accurate simulation of gloss will constitute the subject of this article.

As a matter of fact, our intention is actually much broader. Color and gloss are not two distinct dimensions of appearance, but rather two instances of the same phenomenon. Each of them actually corresponds to specific geometries of illumination and viewing, *45:0*, *d:0* or their reciprocal for color, and near the specular angle for gloss. Rather than concentrating on these specific geometries, what is proposed here is a full goniometric simulation of the spatial distribution of light reflected by a print, which is usually represented by the bi-directional reflectance distribution function (BRDF). The proposed workflow (Figure 1) is essentially an extended version of standard color characterization models. Instead of providing a single output (CIE *XYZ*), it estimates the entire distribution of reflected colors under all possible angles (BRDFs of CIE *X*, *Y* and *Z*).

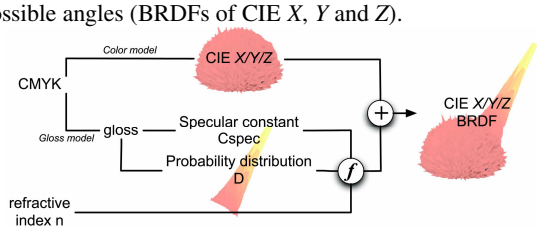

Figure 1. Workflow of the proposed BRDF simulation model. Three identical workflows exist for the CIE X, Y and Z channels.

Goniophotometers cannot realistically be employed in the daily routine of Graphic Arts studios to evaluate prints' BRDFs. Rather, our intent consists of mapping the output of simpler and cheaper instruments, glossmeters and spectrophotometers, to the characteristics of BRDFs. Once all parameters are known, a pixel's BRDF will be simply obtained from this pixel's CMYK coverage.

The first stage of the process consists of mapping CMYK data to CIE *XYZ* and gloss, and will not be detailed here as robust models already exist [11,12]. This article will focus instead on the second stage of the process, how to map gloss and color to BRDF characteristics. An empirical analysis will first unveil the key parameters necessary to model BRDFs. We will then concentrate on finding an accurate mapping between these parameters and measurements of color and gloss. The overall accuracy of the proposed model will finally be evaluated.

Metrology

The BRDF measurements were obtained with Eldim's *EZcontrast* goniophotometer, a remarkable instrument that allows capturing a BRDF in a matter of seconds thanks to the combination of a Fourier lens and a CCD sensor. It can measure the distribution of reflectance in almost the entire hemisphere, i.e. 360 degrees in azimuth and 80 degrees in elevation, with an angular resolution of 0.4 degrees. By using five colored filters, BRDFs in each of the CIE tristimulus values *X*, *Y* and *Z* color bands can be captured. Strictly speaking, it does not measure BRDFs, but reflected radiance. However, a simple normalization by the incoming irradiance can transform the output data into a full-fledged BRDF. The color and gloss measurements were respectively obtained with a GretagMacbeth *Spectrolino* spectrophotometer and a Sheen *Tri-Microgloss Plus 160* glossmeter.

This study aims to offer an accurate rendering of the effect of gloss on all types of printed outputs. Four different types of papers, Xerox *Colortech+ Glossy Coated* (GL), *Premier Matt* (MA), HP *Premium Plus High-gloss* (HI) and *Everyday Semi-glossy* (SE), and two different printers, Xerox *Phaser 7300* and HP *Designjet 20PS*, were chosen to represent standard office output. *National Press* (NA) and *Improved Newsprint* (IM) printed on standard press represent typical newspaper output, while *Coated Satin* (IS) and *DP-Euro Offset gloss* (DP) on inkjet printers represent state-of-the-art printer-based proofing systems.

For each of these papers, BRDF measurements of the 16 combinations of the four primaries at full coverage were performed with an incident light at an elevation of 45 degrees, i.e. replicating the CIE *45:0* geometry. Additionally, measurements of the four primaries at 33% and 66% coverage were obtained, as well as measurements of the cyan colorant illuminated by an incident light at an elevation of 20 degrees and then 70 degrees. Lastly, cyan was also measured with an incident light at an elevation of 45 degrees, as for the first measurement, but with an azimuth of 90 degrees, in order to test for anisotropy. A difference of less than 5% was found and confirmed by a more thorough investigation based on gloss measurements. The small discrepancy was judged not significant and will therefore be ignored in the rest of the analysis. The color characterization was derived from measurements of an IT8.7/3 chart, and from color ramps of each primary for gloss characterization. A summary of the gloss levels recorded for each paper/colorant combinations is shown in the box-and-whisker plot in Figure 3.

Empirical analysis

Figure 2 illustrates some characteristics of the BRDFs of four paper types. A representation of a cyan patch's BRDF illuminated at 45 degrees is shown for each of the CIE tristimulus values *X*, *Y* and *Z*. Due to the exponential nature of the specular lobe, the radiance is plotted on a logarithmic scale. It is evident to observe the radiance is a combination of two components, a diffuse hemisphere and specular lobe. The following analysis will follow this dichotomy.

.

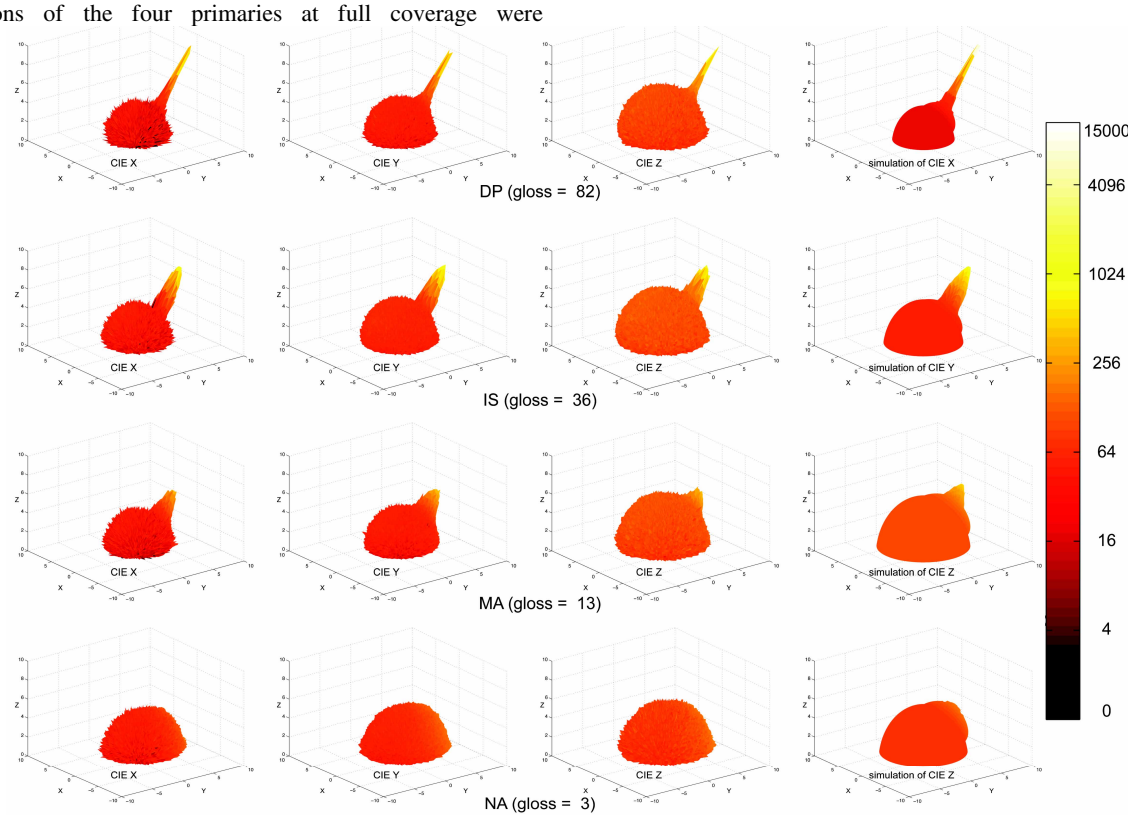

Figure 2. Representation of the BRDFs of papers with gloss levels varying from very glossy (top) to totally mat (bottom). In all cases, the depicted reflectance distributions correspond to a cyan color patch (100 % coverage). In each line are represented (from left to right) the BRDFs of CIE X, Y, Z and finally a simulation of one of these color channels. The incidence of the illuminant is 45 degrees. Due to the exponential nature of the specular lobe, the reflected radiance represented by the color bar is plotted on a logarithmic scale.

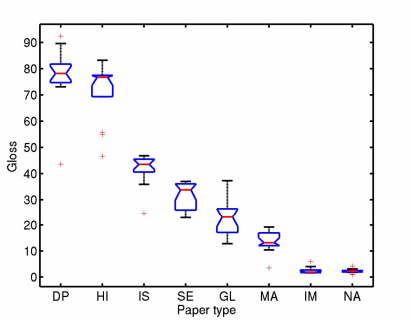

Figure 3. Box-and-whisker plot representing the gloss levels (notably average and differential gloss) of all paper types.

Diffuse component

The diffuse components in Figure 2 are remarkably similar for all paper types regardless of their gloss levels, and are very representative of a typical cyan colorant, made of green and blue, hence the larger *Y* and *Z*. A more surprising feature is that the reflectance distribution of the diffuse component does not follow that of the perfect Lambertian diffuser, as is normally assumed to be the case. If the variations along the azimuthal dimension are not significant, those along the elevation dimension are, as can be seen from Figure 4. As the viewing direction approaches grazing angles, the amount of radiance reflected is quickly diminishing. This phenomenon can be observed for all types of paper and all printed colors.

A two-way ANOVA was realized on the radiance means along azimuthal and elevation dimensions. The obtained p-value for the elevation dimension was zero, which is a very strong indication that a difference exists between the means. This departure from uniformity is however confined to grazing angles and is of little significance compared to the magnitude recorded for the specular lobes. It will therefore be ignored and the diffuse component will be assumed to be Lambertian.

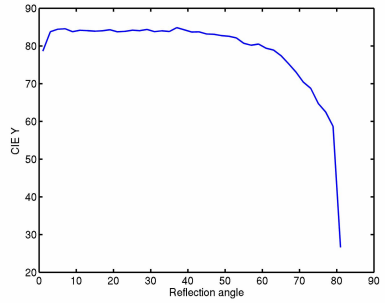

Figure 4. Variation of the reflected radiance as a function of elevation. The figure was derived from the CIE Y BRDF data of a yellow patch printed on DPeuro paper.

Specular component

The specular component is the physical counterpart to gloss, which is an appearance attribute. Measuring gloss consists of estimating the amount of reflected light in a specified angular range defined by the ASTM standards [4]. It should therefore be possible to approximate the glossmeter results from the BRDF measurements by performing a numerical cubature on the appropriate angular range. The corresponding analysis shows a strong correlation between the two sets of results (Table 1, row 1). Note the two types of newsprint paper were omitted from the rest of the analysis because of their lack of specular component.

Width and height of specular lobe

The width and the height of the specular component were found to be loosely correlated to gloss (Table 1, row 2, 3, 4). As expected, an increase in gloss corresponds to an exponential increase in the height of the specular lobe and a linear decrease in its width. The weakness of the correlation may be partially attributed to noise, at least in the width case. The surface of specular component becomes far from smooth as gloss decreases, which results in wide variations in the shape of the best-fitting ellipses and hence the width variations. On the other hand, the height variations observed are of another nature, as explained next.

Table 1. Correlation between gloss measurements and diverse characteristics of the specular lobe of the BRDFs.

	Gloss measurements
Gloss estimated from BRDF	0.968
BRDF lobe width	- 0.875
BRDF lobe height	0.911
Log of BRDF lobe height	0.951

Chromaticity of specular lobe

Contrary to common assumption, the chromaticity of the specular lobe is different from the chromaticity of the illuminant. If the chromaticity of the specular lobe was that of the illuminant, a single point would be seen in Figure 5, but a wide spread can be observed instead. The standard deviations between the chromaticities of the 16 combinations of primaries range between 0.0110 and 0.0581 chromaticity units for each paper type. These are large differences, corresponding to up to 26 ΔE^*_{ab} if the same lightness is assumed. There is no apparent link between the chromaticity of the lobe and the chromaticity of the diffuse component. This confirms the findings published in a recent study. Arney *et al.* [5] establish that a significant amount of specular reflections actually originates from below the surface of a print. Their study reveals the presence of air gaps between colorant and paper, increasing the number of interfaces where Fresnel reflections occur, and thus rationalizing the observed discrepancy.

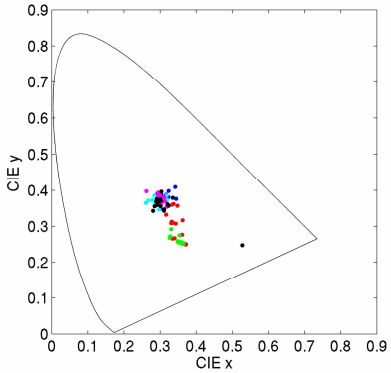

Figure 5. Chromaticities of the specular lobe for all measured colors (16 combinations of the four primaries) and for all papers.

However, our goal is to model the BRDF from a single measurement of gloss. This chromatic information is therefore lost and cannot be reproduced. The model was therefore derived from specular lobes modified to have the chromaticities of the illuminant instead.

Influence of incidence angle

As predicted by the Fresnel equations, the percentage of light reflected specularly increases as a function of the incidence angle of the incoming light (Figure 6). The greater the incidence angle is, the greater the specular reflection becomes and the specular lobe stretches higher.

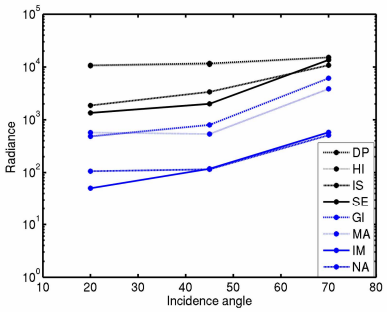

Figure 6. Semi-logarithmic plot of the maximum radiance of the specular lobe as a function of the incidence angle.

BRDF Modeling

The Fresnel equations [6] describe the reflection and refraction processes as a ray of light strikes a boundary, such as the interface between air and matter. They are however only valid for optically smooth surfaces, which never occur in practice. A more complete model of the reflection process for rough surfaces is given by the Kirchhoff theory [7]. It uses a complete physical optics model based on wave theory that takes into account diffraction and interference effects. It is most relevant if the magnitude of the irregularities is comparable to the wavelength of light. Given the object of our study, it is unlikely that such phenomena occur in our case, as the accuracy of the developed model will confirm. In order to describe the scattering of light for surfaces with irregularities larger than light wavelength, models based on geometrical optics offer a much easier approach.

Such models essentially aim at broadening the scope of classical geometric optics by using a statistical approach. A surface is assumed to consist of a collection of micro-facets of different orientation. Because each of these micro-facets behaves like a perfectly reflecting or mirror faces, specular reflections will occur as for an optically smooth surface, i.e. according to Fresnel equations. However, the perturbation generated by the differences in orientation will spread the specular reflections and generate a lobe. These can be described by a probability distribution function of the orientation of the micro-facets, and the one proposed by Beckmann [8] is commonly used.

Many models have been developed based on this theory over the years. However, almost all share a common characteristic. They are dichromatic reflection models, i.e. reflected light is assumed to be a linear combination of two components: surface reflection and sub-surface reflection. We will adopt the model developed by Cook and Torrance [8], as it is the most elaborate and widely used. Alternatively, the equivalent Ward [9] model may also be of interest, as it is computationally faster and handles anisotropic BRDFs. For the sake of clarity, the corresponding equation (Eq. 1) will be kept to its bare minimum by omitting most of the trigonometric terms and the wavelength dependence. The complete equation is widely available [6,7,8].

$$L = C_{diffuse}\cos\vartheta_i + C_{specular}\frac{D(\alpha)\cdot G\cdot F(n)}{\cos\vartheta_r} \qquad (1)$$

As mentioned, the reflectance distribution is approximated as the sum of diffuse and specular components. The diffuse component simply consists of a Lambertian term, i.e. a constant weighted by cosine of the incidence angle of the incoming light. In our approach, this constant will be derived from the color measurements performed with the spectrophotometer. Each tristimulus value will therefore be respectively responsible for the diffuse component of each of the three BRDFs.

As previously mentioned, the specular term is a function of the Fresnel term F, which is itself a function of the index of refraction n of the medium considered. α represents the orientation of a micro-facet relatively to the surface normal, and $D(\alpha)$ the probability distribution function describing the orientation of the micro-facets population (Figure 7). G is a geometrical attenuation factor representing the amount of self-shadowing occurring in rough surfaces. These parameters are weighted by a trigonometric term and a constant that regulates the proportion of diffuse vs. specular reflection.

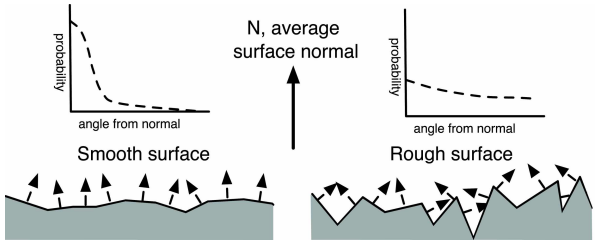

Figure 7. Artistic view of surfaces of different roughness levels approximated by a micro-facet model, with their corresponding probability distribution functions.

This equation contains three unknowns, C_{spec}, $D(\alpha)$ and n, which are all part of the specular term. The task will therefore consist of relating these three constants to the single measurement that describes the specular lobe, gloss. We will proceed in two stages. First, we will first find the parameters that best fit the measured BRDFs using a method developed by Obein [10]. We will them investigate the best ways to map these parameters with the gloss measurements.

Best-fitting parameters

Refractive index n

Let's focus on the specular data in the incidence plane. The product expressed in Equation 2 is independent of the incidence angle, and should therefore be constant for all incidence angles. The refractive index n was obtained by maximizing the overlap between the data measured at incidence angles of 20, 45 and 70 degrees.

$$C_{spec} \cdot D(\alpha) = (L - C_{diffuse} \cos \vartheta_i) \cdot \frac{\cos \vartheta_r}{G \cdot F(n)} \quad (2)$$

The resulting values are displayed in Table 2. Although most are physically plausible (around 1.4 ~ 1.5), some are not (more than 2). Methods such as ellipsometry [6,10] are clearly more indicated to establish the refractive index, and the results presented here should be more considered as numerically optimized parameters rather than physical quantities.

Table 2. Refractive index of all paper types.

	DP	HI	IS	SE	GL	MA	IM	NA
X	2.5	2.5	1.4	1.2	1.3	1.4	1.3	1.5
Y	2.7	2.6	1.4	1.2	1.3	1.4	1.4	1.6
Z	2.6	2.7	1.4	1.2	1.4	1.5	1.6	1.7

Probability distribution D(α) and specular constant C_{spec}

By definition, the integral of the probability distribution function over a hemisphere is equal to $1/2\pi$. Since the refractive index is now known, the product expressed in Equation 2 can be numerically integrated over the hemisphere, and C_{spec} be adjusted in order to make the integral of $D(\alpha)$ equals $1/2\pi$. The resulting C_{spec} values are given in Table 3 and the probability distribution functions $D(\alpha)$ are illustrated in Figure 8.

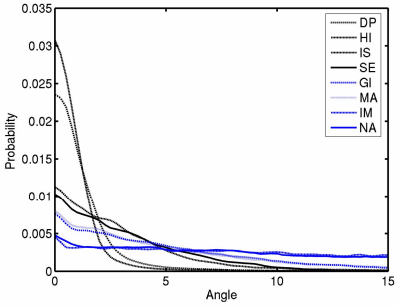

Figure 8. Probability distribution functions of the micro-facets orientation for all papers.

Table 3. C_{spec} values for all paper types, in (lm.m^{-2}.sr^{-1})x10^6.

	DP	HI	IS	SE	GL	MA	IM	NA
X	3.02	2.19	5.67	13.2	3.61	2.05	0.77	0.49
Y	2.49	1.96	6.99	15.9	4.61	2.65	0.73	0.50
Z	2.96	2.14	5.85	14.6	2.66	1.63	0.43	0.36

Relating gloss measurements to BRDF parameters

We have obtained the best fitting parameters representing the measured BRDFs. We will now present how to map them to gloss measurements.

Refractive index n

There is absolutely no connection between the gloss measurements (Figure 3) and the refractive index (Table 2). We therefore cannot predict the latter from the former. However, it is conceivable for the printer / paper / colorant manufacturer to provide such data. We will suppose this is the case and consider the refractive indices as given quantities.

Probability distribution function D(α)

As can be envisioned from Figure 8, the probability distribution functions can be very well approximated by a Gaussian function centered in zero ($R^2 = 0.996$). We thus need to map the characteristics of these Gaussian curves to the gloss measurements. The width of the Gaussian bell is well correlated to gloss ($R^2 = 0.947$), but the height is not. However, the height is very highly correlated to the width ($R^2 = 0.999$). The probability distribution function can therefore be approximated by a Gaussian curve whose parameters are derived from the gloss measurements. The correlation between the estimated and the best-fitting parameters is high ($R^2 = 0.981$).

Specular constant

The height of the specular lobe is determined by the product between the specular constant, the probability distribution function and the Fresnel term. The latter two quantities are now known, and the log of the peak is well correlated to gloss measurements (Table 1, row 4). The specular component is easily obtained from these data. The correlation between the estimated and the best-fitting parameters is good ($R^2 = 0.947$).

Color and gloss characterization models

The second stage of the workflow, whereby color and gloss are mapped to BRDFs parameters, has now been treated. However, the workflow models BRDFs from CMYK data. We therefore need color and gloss characterization models to transform CMYK data into color and gloss values, from which the BRDF parameters will finally be generated.

The model developed by Kuo *et al.* [11] was found to provide an accurate prediction of gloss levels (Table 4). A quadratic polynomial relates the amount of colorant coverage to the level of gloss of this channel, and the final gloss estimation is obtained by a weighted average of each channel's prediction.

A cellular Neugebauer model [12] was used for the color characterization of all paper types. The results can be found in Table 4. The accuracy achieved by both models was judged as satisfactory.

Table 4. Accuracy of color and gloss characterization models. The color errors are expressed in ΔE^*_{00} units and the gloss errors in gloss units.

	DP	HI	IS	SE	GL	MA	IM	NA
Gloss	7.70	5.85	4.10	2.20	8.08	3.74	1.33	1.38
Color	3.09	3.90	3.14	3.83	3.26	3.58	4.63	4.82

Goodness-of-fit of the workflow

The accuracy of the whole workflow was tested by comparing the simulated distribution of radiance to all the measured ones. Results are given in Table 5 and representations of some of the simulated BRDFs are also displayed in the last column of Figure 2. Due to the exponential nature of the specular lobe, it does not make sense to analyze the results in colorimetric terms.

Table 5. Accuracy of the proposed BRDF model for diverse incidences of light. SNR stands for signal-to-noise ratio and is expressed in dB. RMSE stands for root-mean-square error.

		DP	HI	IS	SE	GL	MA	IM	NA
20º	SNR	41.8	37.0	33.3	31.8	28.4	30.1	17.7	19.3
	RMSE	0.86	1.43	2.18	2.59	3.82	3.24	13.0	10.9
	R^2	0.91	0.83	0.93	0.91	0.85	0.92	0.57	0.70
45º	SNR	39.6	37.7	41.2	35.7	32.6	30.3	22.8	21.7
	RMSE	1.07	1.31	0.87	1.64	2.37	3.12	7.27	8.25
	R^2	0.85	0.85	0.97	0.92	0.91	0.88	0.72	0.68
70º	SNR	41.6	41.1	36.5	32.3	31.9	30.0	27.6	28.8
	RMSE	0.84	0.90	1.50	2.43	2.55	3.20	4.24	3.68
	R^2	0.79	0.83	0.91	0.83	0.90	0.84	0.89	0.89

Discussion and Conclusion

The results obtained by the framework outlined above needs to be put into perspective before being analyzed further. Unlike color measurements, noise plays a much greater part in BRDF measurements and comes from various sources. The geometrical configuration of the sample and the measurements are especially important.

On a macroscopic scale, a slight change in geometry will have a significant impact on the data forming the specular lobe, whereas color measurements are oblivious to it. Even the slightest rotation of the sample being measured will modify the lobe's spatial location. Its width will also be significantly affected by any bend present in the sample. For reference, the two glossiest papers measured here have a specular lobe whose width is less than two degrees at mid-height. The angular resolution of the goniophotometer is also of crucial importance in such cases.

Even if quality of the measurement geometrical configuration can be guaranteed, small altitude variations exist at the surface of the paper on a mesoscopic scale. When gloss is considered, a print cannot be considered as flat, and different radiance distributions will be recorded in different part of the print, even if it only contains a single uniform color patch. This phenomenon is known as microgloss [13, 14].

In that context, the accuracy achieved by the proposed model can be considered at the very least as good. The results for the six glossy papers are particularly satisfactory. Although the correlation between simulated and measured data is not always greater than 0.9, a visual inspection of the radiance distributions shows the overall width and height of the lobe is very well respected by the model. The signal-to-noise ratio is almost always higher than 30dB, and sometimes even higher than 40 dB, which is excellent. Difficulties in controlling the geometrical configuration of a sample definitely lead to reducing the overall accuracy. A second contributing factor consists of the singularity of the gloss measurement, which cannot render the chromatic diversity of the specular component and hence the differences in height between channels. Lastly, the diffuse component is also affected, which is especially crucial because, for any of the glossy papers, it represents more than 99% of the total hemispherical distribution. As previously mentioned, the diffuse component does not behave strictly speaking as a perfectly Lambertian diffuser, and inter-instrument agreement issues, whereby two color measurement instruments are unlikely to concur, further impair the proposed simulation.

In absolute terms, the accuracy of the simulation for the six glossy papers can be considered as good, and even better if all the mentioned issues are taken into account. However, the figures suggest the precision obtained for matt papers is much lower. Even if low radiance magnitudes characteristic of matt samples amplifies this lack of precision, there is no denying that the proposed model offers no more than an approximate simulation of matt reflections. The model scales down from very high to intermediate to very low gloss in a very graceful manner, but not quite all the way to totally matt samples. This could provide the starting point for further improvement to the proposed model. We however feel that incorporating microgloss effects into the equation would be of much greater value. As emphasized in this article, gloss is all about geometry, unlike color. Any gloss simulation will be incomplete without modeling the small variations present on a mesoscopic scale.

Acknowledgement

We would like to Françoise Viénot and Nacim Ladjouze from the Centre de Recherches sur la Conservation des Documents Graphiques, Muséum National d'Histoire Naturelle (Paris) for allowing access to the EZContrast, their tremendous help in performing the measurements as well as the very kind reception, Gael Obein for the pertinent advices on correctly implementing his method, and Chris Grawe from Keene Repro Ltd (London) for supplying a superb sets of samples. Alexis would also like to thank the reviewers for their great suggestions and last but not least Yazhu Ling for painstakingly reviewing the early drafts of this article.

References

[1] IPA, 2005 IPA Color Proofing RoundUP Special Report, www.ipa.org (2005).
[2] ISO, ISO 3664 Viewing conditions – Graphic technology and photography (2000).
[3] ISO, ISO 12646 Graphic technology—Displays for colour proofing—Characteristics and viewing conditions (1999).
[4] ATSM, ASTM D523-89(1999) Standard Test Method for Specular Gloss, ASTM International Standards on Color and Appearance Management (1999).
[5] J.S. Arney, P.G. Anderson and W. Pfeister, Color Properties of Specular Reflections, Proc. NIP20 (2004).
[6] A.S. Glassner, Principles of Digital Image Synthesis (Kaufmann) (1995).
[7] A. Watt and M. Watt, Advanced Animation and Rendering Techniques (Addison-Wesley), (1998).
[8] R.L. Cook and K.E.Torrance, A Reflectance Model for Computer Graphics, Computer Graphics, 15(3), (1981).
[9] G.J. Ward, Measuring and modeling anisotropic reflection, Proc. SIGGRAPH92, 26(2), (1992).
[10] G. Obein, Caracterisation optique et visuelle du brilliant, PhD thesis (2003).
[11] C. Kuo, Y. Ng and J.C. Wang, Differential Gloss Visual Threshold Under Normal Viewing Conditions, Proc. NIP18, (2002).
[12] R. Bala, Chapter 5: Device Characterization, in Digital Color Imaging Handbook, G. Sharma (ed.), (2002).
[13] P. Hansson, Simulation of small-scale gloss variations based on topographic data (unknown origin).
[14] Y. Ng, E. Zeise, D. Mashtare, J. Kessler, J. Wang, C. Kuo, E. Maggard and P. Mehta, Standardization of Perceptual Based Gloss and Gloss Uniformity for Printing Systems, PICS Conf. (2003).